Phase boundary in the dimensionality of angle-dependent magnetoresistance oscillations in the charge-transfer salt $\alpha - (BEDT - TTF)_2KHg(SCN)_4$

1996 J. Phys.: Condens. Matter 8 8829

(http://iopscience.iop.org/0953-8984/8/45/017)

J. Phys.: Condens. Matter **8** (1996) 8829–8845. Printed in the UK

Phase boundary in the dimensionality of angle-dependent magnetoresistance oscillations in the charge-transfer salt α-(BEDT-TTF)$_2$KHg(SCN)$_4$

A A House†, S J Blundell†, M M Honold†, J Singleton†,
J A A J Perenboom‡, W Hayes†, M Kurmoo†§‖ and P Day§

† Department of Physics, University of Oxford, Clarendon Laboratory, Parks Road, Oxford OX1 3PU, UK

‡ Laboratorium voor Hoge Magneetvelden, Katholieke Universiteit Nijmegen, Toernooiveld 1, NL 6525 ED Nijmegen, The Netherlands

§ The Royal Institution, 21 Albemarle Street, London W1X 4BS, UK

Received 10 June 1996, in final form 4 July 1996

Abstract. Angle-dependent magnetoresistance oscillations (AMROs) have been studied in the isostructural charge-transfer salts α-(BEDT-TTF)$_2$KHg(SCN)$_4$ and α-(BEDT-TTF)$_2$NH$_4$Hg(SCN)$_4$ (where BEDT-TTF is bis(ethylenedithio)tetrathiafulvalene) in steady fields of up to 30 T. The shapes of the approximately elliptical quasi-two-dimensional (Q2D) Fermi surfaces that these organic metals possess have been determined at 30 T and are found to be in broad agreement with recent band-structure calculations. The Fermi surface of the salt α-(BEDT-TTF)$_2$KHg(SCN)$_4$ undergoes a reconstruction at low fields and temperatures, resulting in a change in the dimensionality of the AMROs from Q2D character to quasi-one-dimensional character. This change is associated with the kink transition that is observed in magnetic field sweeps and is attributed to the formation of a spin-density wave ground state. The phase boundary of the change in the AMRO dimensionality has been followed to both the low-temperature high-field (about 23 T) and low-field high-temperature (about 8 K) extremes. The data are compared with recently proposed models of the AMROs and Fermi surfaces for these materials.

1. Introduction

Charge-transfer salts of the type (BEDT-TTF)$_n$X, where BEDT-TTF is bis(ethylenedithio) tetrathiafulvalene, exhibit diverse low-temperature ground states including superconducting, charge-density wave and spin-density wave (SDW) states [1]. In these materials the BEDT-TTF molecules stack alongside one another in layers which are partitioned by sheets of the anion X. Within the BEDT-TTF layer there is overlap of the molecular π orbitals between neighbouring molecules which gives rise to quasi-two-dimensional (Q2D) metallic conduction.

One interesting subset of this family of salts is an isostructural class of organic conductors of the form α-(BEDT-TTF)$_2$MHg(SCN)$_4$, where M = K [2], Tl [3], Rb [4] or NH$_4$ [5]. The first band-structure calculations for these salts were carried out by Oshima *et al* and predicted almost identical Fermi surfaces consisting of a Q2D closed hole pocket

‖ Present address: Institut de Physique et Chimie des Matériaux de Strasbourg, 23 rue du Loess, BP 20/CR, F-67037 Strasbourg, France.

0953-8984/96/458829+17$19.50

and a pair of quasi-one-dimensional QID sheets (figure 1(*c*)) [5]; the close similarity was not unexpected, owing to the isostructural nature of the α-phase salts. In spite of this the salt α-(BEDT-TTF)$_2$NH$_4$Hg(SCN)$_4$ has a superconducting ground state with $T_c \simeq 1$ K, while the salts with M = K, Rb or Tl show a transition to an antiferromagnetically ordered state below $T_N \simeq 8$–10 K [6] and remain metallic down to less than 100 mK [7]. A wide variety of experimental probes of the transition at T_N have led to the proposal that it represents the onset of a SDW state (see [8] and references therein).

The availability of high-quality crystals has enabled a large number of experimental studies of the Shubnikov–de Haas (SdH) [9, 10] and de Haas–van Alphen (dHvA) [11, 12] oscillations which occur in the resistance and magnetization, respectively, of these salts at low temperatures. The salt α-(BEDT-TTF)$_2$NH$_4$Hg(SCN)$_4$ exhibits monotonically increasing magnetoresistance and only a single series of quantum oscillations of frequency $F_\alpha \simeq 567$ T. This series has been identified with the Q2D hole pocket of the Fermi surface (figure 1(*c*)). In contrast, the salts with M = K, Tl and Rb display a pronounced hump in their magnetoresistance and multiple series of quantum oscillations in the region below a characteristic field known as the 'kink' field B_k [13]. Comparative traces of the magnetoresistance of α-(BEDT-TTF)$_2$NH$_4$Hg(SCN)$_4$ and α-(BEDT-TTF)$_2$KHg(SCN)$_4$ are presented in figures 1(*a*) and 1(*b*). The kink field occurs at about 23 T in the case of α-(BEDT-TTF)$_2$KHg(SCN)$_4$, being manifested as a sharp drop in magnetoresistance. Above this field the magnetoresistance of this material increases monotonically and consists of only one SdH frequency, $F_\alpha \simeq 670$ T. The behaviour of α-(BEDT-TTF)$_2$KHg(SCN)$_4$ above the kink field thus resembles that of α-(BEDT-TTF)$_2$NH$_4$Hg(SCN)$_4$.

One interpretation [14] of the kink transition suggests that it corresponds to the point at which the applied magnetic field overwhelms the antiferromagnetic ordering of the low-temperature ground state. Below the kink field it has been proposed that the periodic potential associated with the SDW causes the Q1D sheets of the calculated Fermi surface of Oshima *et al* (figure 1(*c*)) to nest, leading to a reconstructed Fermi surface of the form shown in figure 1(*d*) [14]. This Fermi surface consists of small Q2D pockets separated by strongly corrugated Q1D Fermi surface sheets that are inclined at an angle of about 21° to the crystalline $\boldsymbol{b}$–$\boldsymbol{c}$ plane. At the kink field it has been proposed [10] that the Fermi surface reverts to the form of figure 1(*c*) leading to the recovery of magnetoresistance akin to that of α-(BEDT-TTF)$_2$NH$_4$Hg(SCN)$_4$.

While this model of the α-(BEDT-TTF)$_2$MHg(SCN)$_4$ salts has been successful in describing certain aspects of the observed quantum oscillatory phenomena, it certainly does not provide a complete explanation of the low-temperature low-field ground state. In particular it does not adequately account for the complexity of the SdH waveform below the kink transition [13]. The context in which it has been most successfully utilized (and that in which it was originally proposed) is in the study of angle-dependent magnetoresistance oscillations (AMROs).

AMROs are measured by recording the resistance of a crystal of (BEDT-TTF)$_n$X as a function of the angle θ between its crystalline $\boldsymbol{b}^*$ axis and a constant external magnetic field. There are two types of AMRO that have been observed in the α-(BEDT-TTF)$_2$MHg(SCN)$_4$ family of salts, both of which are periodic in the tangent of θ. The first are found in the low-temperature SDW state of the M = K, Rb and Tl materials [10, 14]. These AMROs originate from the Q1D sheets of the Fermi surface and are manifested as sharp *minima* in the sample resistance. The other type of AMRO has been observed in α-(BEDT-TTF)$_2$NH$_4$Hg(SCN)$_4$ [15] and has its origins in Q2D sections of Fermi surface [16]. These AMROs consist of pronounced *maxima*. In α-(BEDT-TTF)$_2$MHg(SCN)$_4$ the AMROs have been shown to undergo a transition between Q1D behaviour in the low-field low-temperature SDW state

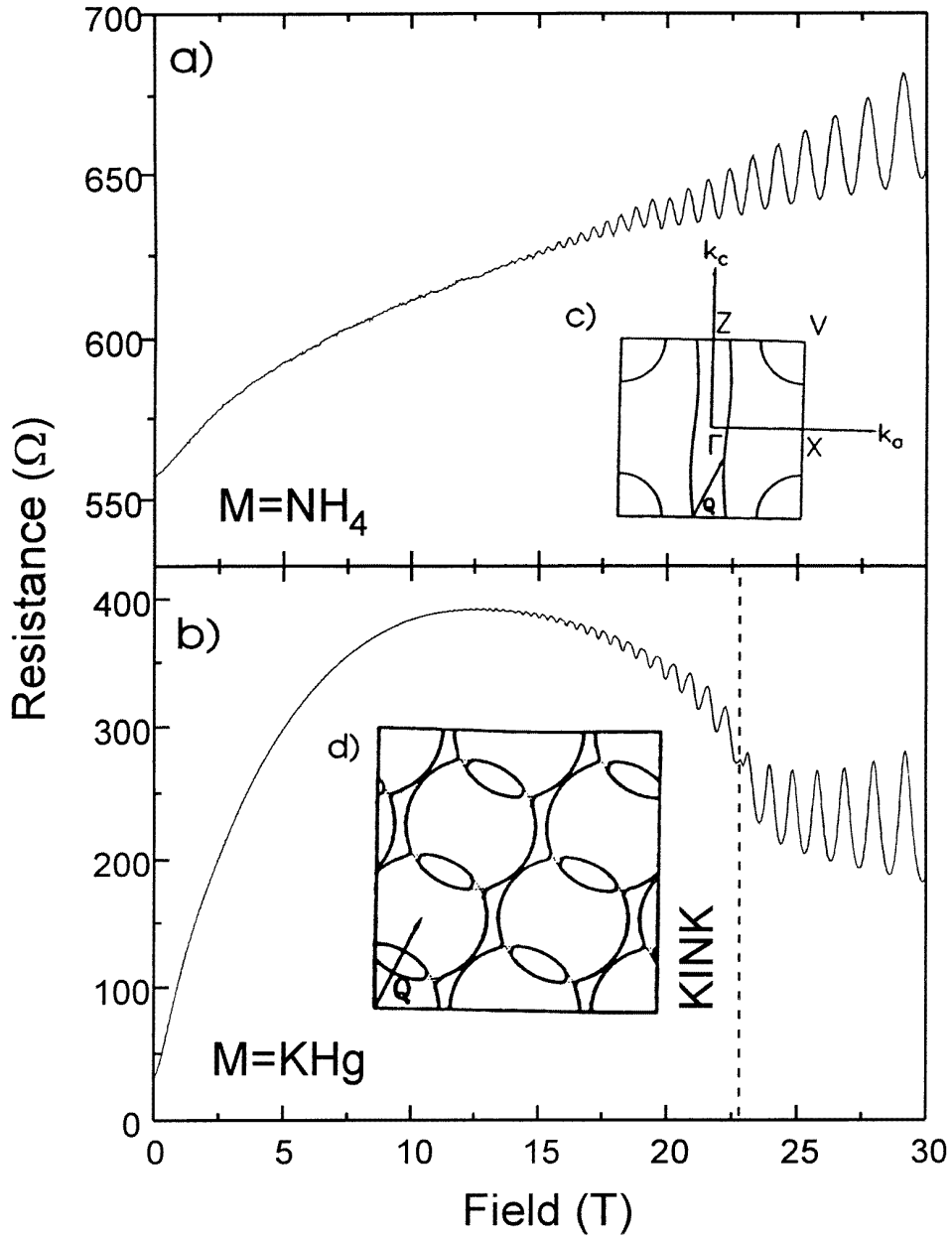

Figure 1. (*a*) Magnetoresistance of α-(BEDT-TTF)$_2$NH$_4$Hg(SCN)$_4$ with the current directed perpendicular to the ***a*–*c*** plane at 1.4 K. (*b*) Magnetoresistance of α-(BEDT-TTF)$_2$KHg(SCN)$_4$ with the current directed perpendicular to the ***a*–*c*** plane at 1.4 K. (*c*) Calculated Fermi surface from [2]. (*d*) Nested Fermi surface from [14].

to Q2D behaviour outside this state. This change in the AMRO dimensionality has been observed in α-(BEDT-TTF)$_2$KHg(SCN)$_4$ as a function of *temperature* in fields of 14 T by Kovalev *et al* [17] and as a function of *field* at a temperature of 1.5 K by Caulfield *et al* [10] and Sasaki and Toyota [18]. Recently Hanasaki *et al* [19] have shown that a similar change

occurs in the AMROs of α-(BEDT-TTF)$_2$KHg(SCN)$_4$ as a function of applied *pressure*, the transition taking place at about 5 kbar.

On the basis of the above results the phase boundary depicted in figure 2 has been proposed for the low-temperature (SDW) state of α-(BEDT-TTF)$_2$KHg(SCN)$_4$ [19, 20]. Recent data reported by Sasaki and Toyota [21] have, however, led to the suggestion of a more elaborate field–temperature (B–T) phase diagram in which the high-temperature and high-field states are not identical. AMRO studies by Kartsovnik *et al* [22] have also indicated that these two regions of the B–T phase diagram may be dissimilar. Caulfield *et al* [10] mapped out the shape of the Q2D Fermi surface pocket in α-(BEDT-TTF)$_2$KHg(SCN)$_4$ at 24 T and 1.5 K and found that its size and ellipticity were similar to the high-temperature pocket of Kovalev *et al* [17] but that its orientation differed by approximately 90°. (The major axis of the ellipse found by Kovalev *et al* lies at a shallow angle to the reciprocal-space $\boldsymbol{k}_a$ axis while that obtained by Caulfield *et al* lies at a similar angle relative to the $\boldsymbol{k}_c$ axis.) This discrepancy is addressed later in this paper. Recently, a pulsed field measurement of the dHvA effect in α-(BEDT-TTF)$_2$KHg(SCN)$_4$, in fields of up to 54 T [12], has shown that the kink transition is broader in field than had previously been thought and is not fully completed until about 27 T. In the light of this result it is questionable whether the 24 T data of Caulfield *et al* are truly representative of the high-field regime, and therefore it is necessary to investigate the B–T phase boundary of the AMRO dimensionality in order to ascertain whether the high-temperature and high-field regimes are identical. In this paper we present measurements of the AMROs of a single crystal of α-(BEDT-TTF)$_2$KHg(SCN)$_4$ for 1.4 K < T < 9 K and 5 T < B < 30 T. We have also measured Q2D AMROs in α-(BEDT-TTF)$_2$NH$_4$Hg(SCN)$_4$ up to 30 T and we discuss these results in relation to those obtained for α-(BEDT-TTF)$_2$KHg(SCN)$_4$.

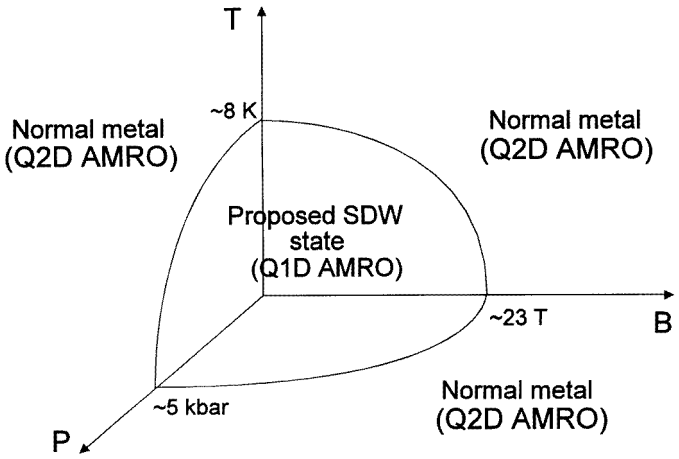

Figure 2. Pressure–temperature–field phase diagram for the SDW state in α-(BEDT-TTF)$_2$KHg(SCN)$_4$.

2. Experimental method

Two single-crystal samples of α-(BEDT-TTF)$_2$KHg(SCN)$_4$ and α-(BEDT-TTF)$_2$NH$_4$Hg(SCN)$_4$ were prepared using standard electrochemical techniques [23]. The resultant black platelets each had 25 μm gold wires attached with platinum paint to the faces cor-

responding to their crystalline $\boldsymbol{a}$–$\boldsymbol{c}$ planes. Standard four-wire AC techniques (90–130 Hz) were then used to measure the sample resistance with the current (5–10 μA) in the direction of the crystalline $\boldsymbol{b}$ axis. Magnetoresistance measurements were carried out using a cryogenic insert that enabled the sample to be rotated about two perpendicular axes with a precision of $\pm 1^\circ$. Measurements at T > 4.2 K were performed in a ^{4}He flow cryostat in a 17 T Bitter magnet at the University of Nijmegen. Fields of up to 30 T were provided by the Bitter magnets at the National High Magnetic Field Laboratory, Tallahassee. The same α-(BEDT-TTF)$_2$KHg(SCN)$_4$ crystal was used throughout the experiment although it was remounted between the Nijmegen and Tallahassee data-taking runs. The sample orientations were determined by polarized infrared reflectivity at room temperature [24].

3. Experimental data

3.1. α-(BEDT-TTF)$_2$KHg(SCN)$_4$

In figure 3(*a*) the temperature dependence of the AMROs in α-(BEDT-TTF)$_2$KHg(SCN)$_4$ is shown for a field of 14 T. These data were recorded at an azimuthal angle of $\phi = +40^\circ$, where rotation with the magnetic field vector in the crystalline $\boldsymbol{a}$–$\boldsymbol{b}$ plane is defined to be at $\phi = 0^\circ$. At this field the 4.1 K data lie well within the low-temperature SDW state and exhibit clear minima, indicative of the presence of Q1D Fermi surface sheets. As the temperature rises, it is seen that the form of the AMROs changes from one of a gently curving background with superposed sharp minima to one where the background has pronounced maxima superposed upon it. Note that the large central maximum (near $\theta = 0^\circ$) in the low-temperature data becomes a minimum above 7 K.

Figure 3(*b*) shows the progression of the AMROs as a function of field at a constant temperature of 6 K, and at the same azimuthal angle ($\phi = +40^\circ$) as that in figure 3(*a*). It is apparent that the 13 T trace in figure 3(*b*) bears a strong resemblance to the 4.1 K trace of figure 3(*a*), i.e. it is Q1D in nature. As the field applied to the sample is increased, it is clear that a change in the character of the AMROs analogous to that in figure 3(*a*) occurs, with the AMRO dips being removed while peaks appear. Again the central AMRO maximum at low fields inverts and becomes a minimum at higher fields.

The change in the dimensionality of the AMROs from Q1D to Q2D demonstrates a significant rearrangement of the Fermi surface between the low-field low-temperature SDW state and the 'normal' metallic state. In particular we shall use the behaviour of the AMROs near $\theta = 0^\circ$ to define the phase boundary; a convex maximum will be taken to represent the Q1D AMRO state, and a concave minimum the Q2D AMRO state. This change from convexity to concavity is reflected in the sharp change in the magnetoresistance of α-(BEDT-TTF)$_2$KHg(SCN)$_4$ (figure 1(*b*)) from negative to positive at the kink transition which occurs at about 23 T. AMRO traces for 5 T < B < 30 T (figure 4) show that this agrees well with the observed change in the AMRO dimensionality. Furthermore the dimensionality change exhibited by the data in figure 3 is seen to agree well with the phase boundary for the SDW state proposed in [21].

It is seen in the 30 T data in figure 4 that, even at this high field, the AMROs close to $\theta = \pm 90^\circ$ appear unchanged from these occurring at similar large angles but at fields well below 23 T. This supports the suggestion of Caulfield *et al* [10] that the SDW state persists at these angles even at high fields. The 30 T AMROs at $-75^\circ < \theta < +75^\circ$ are unambiguously of Q2D character with large SdH oscillations of fundamental frequency about 670 T superimposed upon it. At tilt angles of about 70° on either side of the trace the peaks have the appearance of occurring in pairs (i.e. it looks like each AMRO peak splits

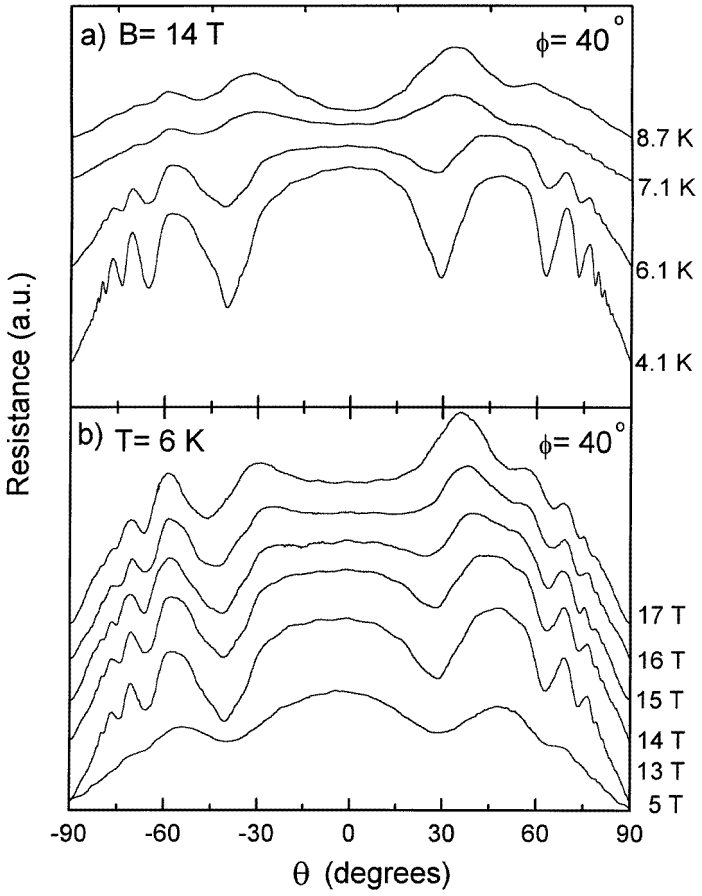

Figure 3. (*a*) Temperature dependence of the AMROs in α-(BEDT-TTF)$_2$KHg(SCN)$_4$ at 14 T, showing the change from Q1D to Q2D character. θ is defined as the angle between the crystal $\boldsymbol{b}^*$ axis and the external magnetic field while ϕ is an azimuthal angle where rotation with the magnetic field vector in the crystalline $\boldsymbol{a}$–$\boldsymbol{b}$ plane is defined to be at $\phi = 0^\circ$. (*b*) Field dependence of the AMROs across the phase boundary in α-(BEDT-TTF)$_2$KHg(SCN)$_4$ at 6 K.

into two separate peaks). In spite of this, plots of the peak periodicity in $\tan\theta$ (figure 8(*a*)) against index n confirmed that they are separate Q2D peaks.

The AMROs were also studied as a function of the azimuthal angle ϕ at a variety of fields and temperatures. Full ϕ dependences were performed for the Q2D regime at 7.1 K, 14 T, and 1.4 K, 30 T and for the Q1D regime at 5.9 K, 5 T, and 1.4 K, 20 T. Representative traces of this work, taken at 1.4 K, are presented in figure 5.

3.2. α-(BEDT-TTF)$_2$NH$_4$Hg(SCN)$_4$

In figure 6(*a*) the variation in the AMROs with field is presented for α-(BEDT-TTF)$_2$NH$_4$Hg(SCN)$_4$ at 1.4 K and $\phi = +80^\circ$ (ϕ is again defined to be zero for rotation in the $\boldsymbol{a}$–$\boldsymbol{b}$ plane). A single series of Q2D AMROs is observed for this material at all fields. Further peaks on the trace occur at high fields owing to the presence of SdH oscillations occurring as the field is swept through θ and have their largest amplitude near

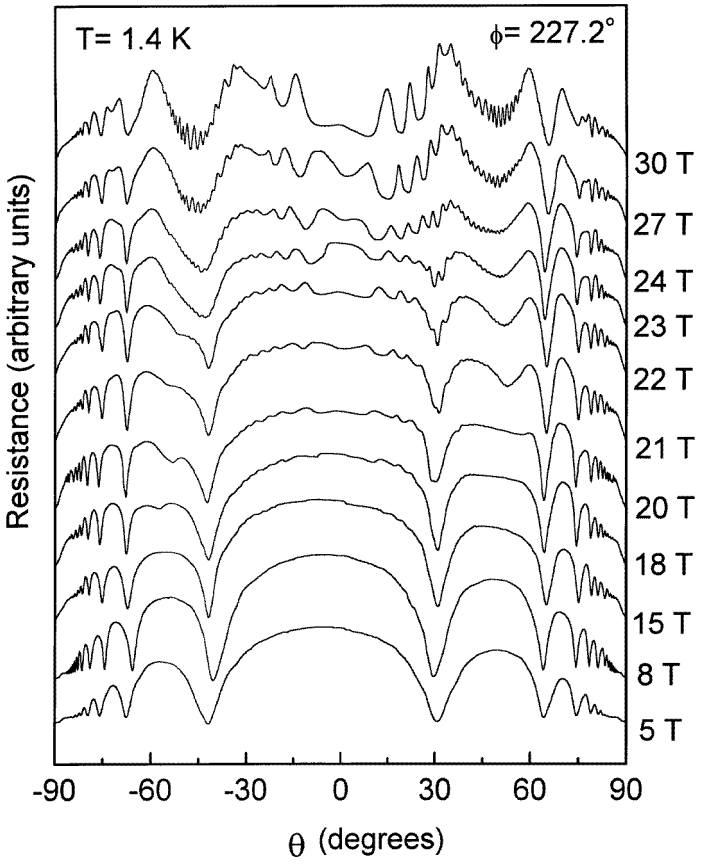

Figure 4. Field dependence of the AMROs in α-(BEDT-TTF)$_2$KHg(SCN)$_4$ at 1.4 K showing the change in dimensionality at about 23 T.

$\theta = 0$. No change in the dimensionality of the AMROs is observed across the field range. (The peak near $\theta = 0$ in the 30 T data is attributable to a SdH oscillation.) The ϕ dependence of the α-(BEDT-TTF)$_2$NH$_4$Hg(SCN)$_4$ AMROs was measured at 30 T and 1.4 K (figure 6(*b*)).

4. Discussion

4.1. α-(BEDT-TTF)$_2$KHg(SCN)$_4$

We have applied the criterion of convexity or concavity near $\theta = 0$ to distinguish between Q1D and Q2D AMROs, respectively, and show the change in dimensionality in figure 7, in which the full squares represent Q1D AMRO traces, and the full triangles Q2D traces. The broken curve represents the phase boundary proposed in [21]. This curve takes the form

$$T(B) = T_{SDW}[1 - (B/B_{SDW})^2]^{1/2} \tag{1}$$

where $T_{SDW} = 8$ K and $B_{SDW} = 23$ T are fitting parameters determined so as to fit the temperature dependence of the kink transition as observed in magnetoresistance

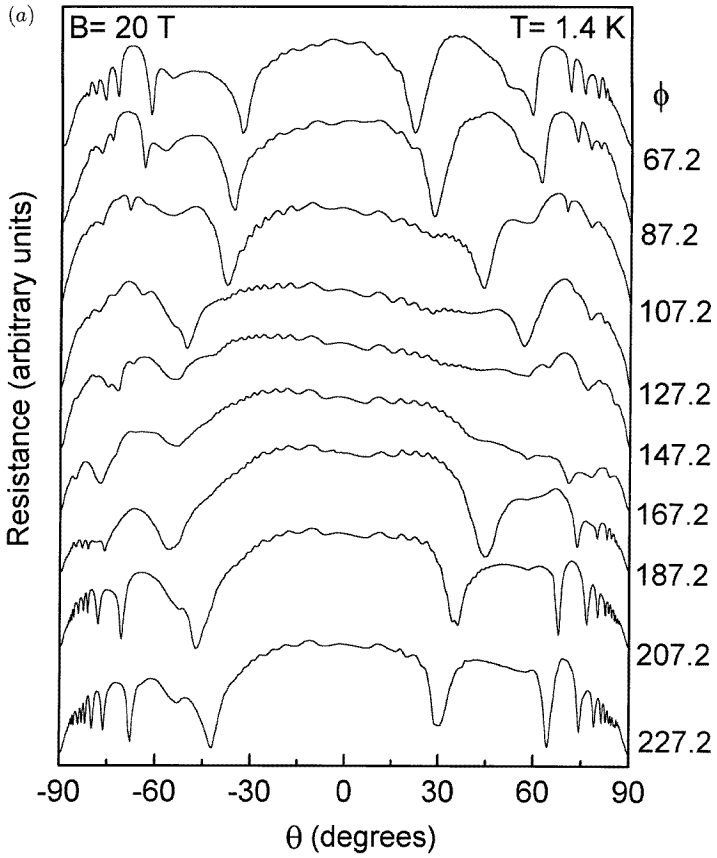

Figure 5. (*a*) ϕ dependence of the Q1D AMROs in α-(BEDT-TTF)$_2$KHg(SCN)$_4$ at 20 T and 1.4 K. (*b*) ϕ dependence of the Q2D AMROs in α-(BEDT-TTF)$_2$KHg(SCN)$_4$ at 30 T and 1.4 K.

measurements presented in that reference. Thus the phase boundary of the transition in the AMRO dimensionality is conclusively identified with the kink transition.

The data points A–D in figure 7 are points at which a full ϕ dependence of the AMROs was measured. The ϕ dependence of the data taken at point A (20 T, 1.4 K) is shown in figure 5(*a*). This point lies within the low-temperature low-field region of the α-(BEDT-TTF)$_2$KHg(SCN)$_4$ *B–T* phase diagram and it is clear from figure 5(*a*) that the AMROs at this point are Q1D in character. Moving from point A to point B (30 T, 1.4 K) involves crossing the phase boundary so that the data taken at point B are Q2D in character. Figure 5(*b*) shows the ϕ dependence of the AMROs at point B. Comparison of this figure with figure 5(*a*) highlights the differences between the two types of AMRO.

4.1.1. Quasi-one-dimensional oscillations. The theory of Q1D AMROs has been dealt with by numerous workers [25], especially in the context of TMTSF-based organic conductors. Recently a semiclassical description of Q1D AMROs has been developed and successfully used to model the AMROs and magnetoresistance in the low-temperature low-field state of α-(BEDT-TTF)$_2$KHg(SCN)$_4$ [26]. This model describes the periodicity of the Q1D

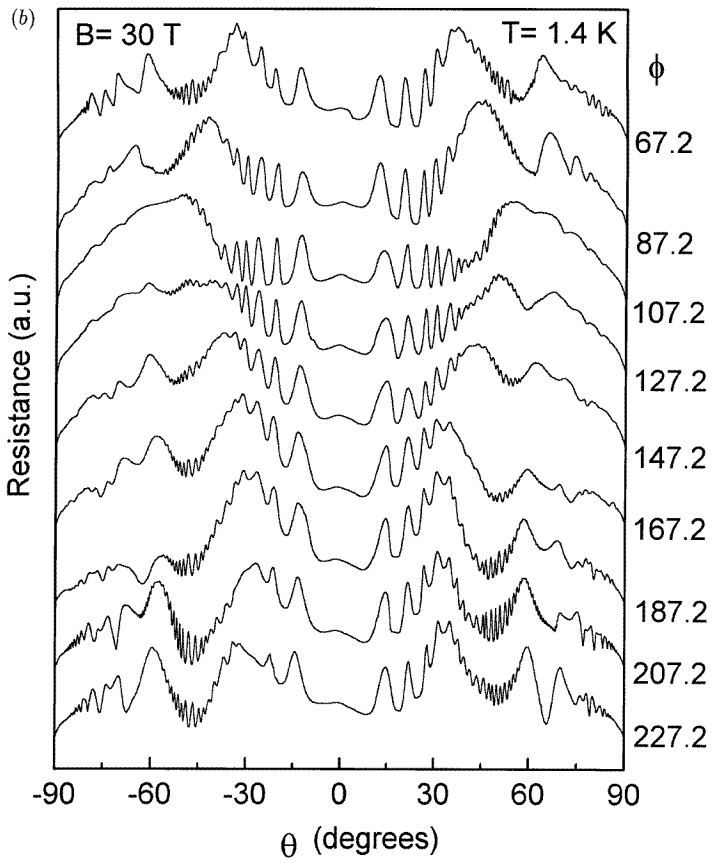

Figure 5. (Continued)

AMROs, for a general case, by the equation

$$\tan\theta = \frac{mb}{nc} + \frac{d}{c} \tag{2}$$

in which m and n are non-zero integers, b and c are parameters that quantify the fundamental periodicity of the Fourier components of the warping of the Q1D Fermi surface sheets in two perpendicular directions within the plane of the sheets and d parametrizes the obliquity of the Fermi surface warping. At the θ-values identified in equation (2), resonances in the conductivity occur (and hence sharp resistance minima). In α-(BEDT-TTF)$_2$KHg(SCN)$_4$ the Fermi surface corrugation has very high harmonic content within the $\boldsymbol{a}$–$\boldsymbol{c}$ plane because it is formed by joining together sections of warped cylinder [26]. The dominant magnetoresistance resonances that occur in this special case have $|n| \leqslant 1$. For this reason in the experimental data no 'fractional' AMROs are observable and equation (2) simplifies to the form

$$\tan\theta = \chi\nu + \kappa \tag{3}$$

where χ and κ are constants and $\nu = \ldots, -2, -1, 0, +1, +2, \ldots$.

By plotting the position of Q1D AMRO minima in $\tan\theta$ space against the integer index the value of χ was thus obtained as a function of ϕ for point A (20 T, 1.4 K) and point C

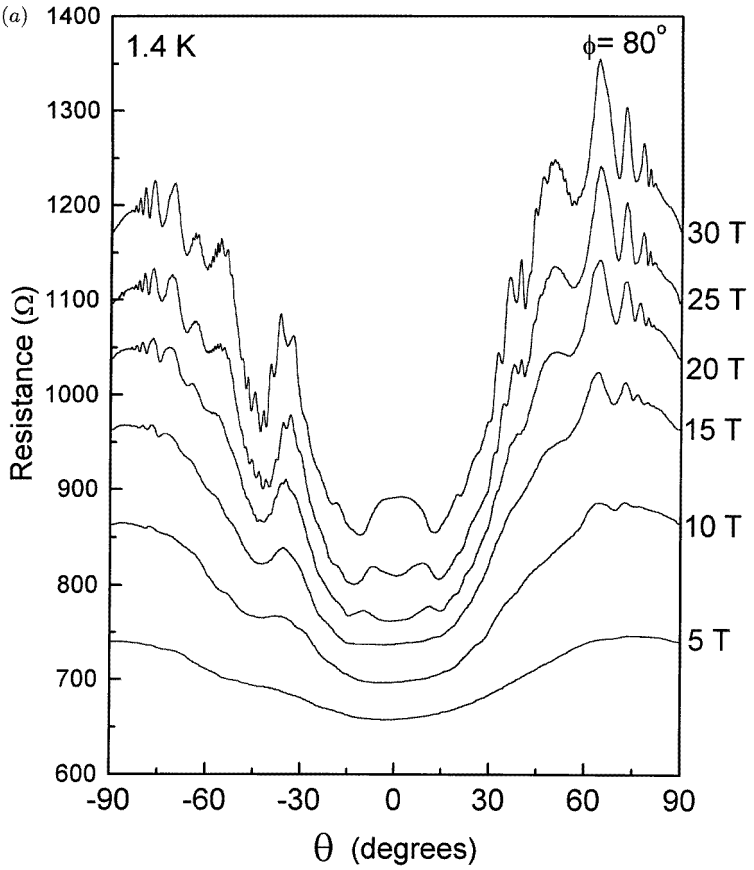

Figure 6. (*a*) Field dependence of α-(BEDT-TTF)$_2$NH$_4$Hg(SCN)$_4$ AMROs at 1.4 K. (*b*) ϕ dependence of α-(BEDT-TTF)$_2$NH$_4$Hg(SCN)$_4$ AMROs at 30 T and 1.4 K: a.u., arbitrary units.

(5 T, 5.9 K). The azimuthal angular dependence of χ for the data taken at point C was fitted to the equation

$$\chi(\phi) = \frac{\chi_0}{\cos(\phi - \phi_0)} \tag{4}$$

with fitting parameters $\chi_0 = 1.26 \pm 0.03$ and $\phi_0 = (+65.7 \pm 1)^\circ$, in good agreement with earlier work [10, 15, 17, 18]. The measurement at point C was performed at Nijmegen after which the crystal axes of the α-(BEDT-TTF)$_2$KHg(SCN)$_4$ crystal used in this experiment were determined. The crystal was remounted on its sample holder prior to the measurement at point A, which was carried out at Tallahassee. The value of ϕ_0 obtained at point C was then used to determine the orientation of the crystal after it had been remounted by *defining* ϕ_0 to be $\phi_0 = +65.7^\circ$ on the data taken at Tallahassee. Low-field low-temperature AMRO measurements were carried out during the work at both Nijmegen and Tallahassee, and identical results were obtained for the two cases. This method of alignment assumes that the direction of the Q1D Fermi surface sheets remains constant across the low-temperature low-field state and is independent of sample cooling conditions. This assumption is supported by previous AMRO measurements [10, 17] and polarized infrared reflectivity measurements

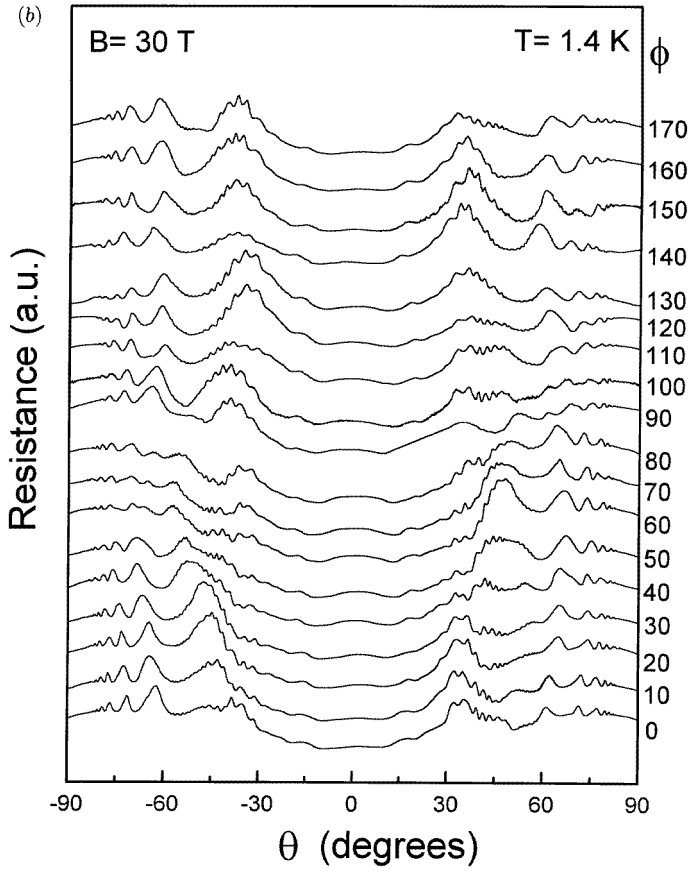

Figure 6. (Continued)

that we performed upon the crystal subsequently to the work at Tallahassee. For point A we found that $\chi_0 = 1.31 \pm 0.03$.

4.1.2. Quasi-two-dimensional oscillations. Q1D AMROs are most pronounced when the Fermi surface sheets giving rise to them are strongly corrugated [26]. In contrast, Q2D AMROs are more dominant when the warping of the Fermi surface cylinders that they originate from are only slightly warped. It is for these reasons that the nested Fermi surface of α-(BEDT-TTF)$_2$KHg(SCN)$_4$ exhibits Q1D AMROs. In that case the Q1D Fermi surface sections have been formed from the remnants of the Fermi surface cylinders of the unreconstructed Fermi surface and so the Fermi surface corrugations are quite cusp like, i.e. they have a high harmonic content. In the 'normal' metallic state of α-(BEDT-TTF)$_2$KHg(SCN)$_4$ the Q1D Fermi surface sheets that are present are much smoother than in the reconstructed Fermi surface and in this circumstance the AMROs become dominated by those originating from the Q2D Fermi surface cylinders.

In this section we consider the Q2D AMROs recorded at points B and D. Point B lies well within the 'normal' metallic regime and corresponds to the data in figure 5(*b*). Q2D AMROs are connected with the vanishing of the electronic group velocity perpendicular to the $\boldsymbol{a}$–$\boldsymbol{c}$ plane when a warped Q2D Fermi surface cylinder is tilted at special angles to the

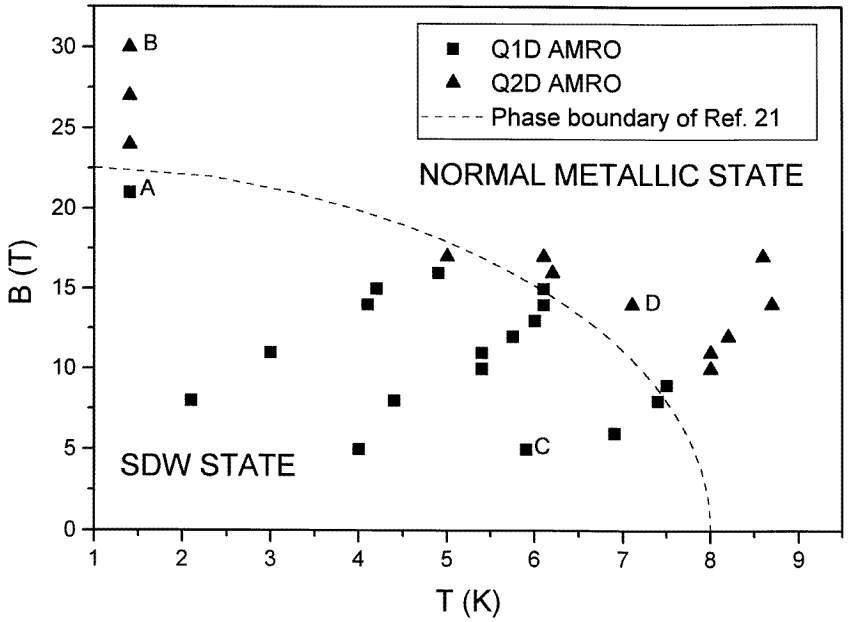

Figure 7. The phase boundary of the AMRO dimensionality in α-(BEDT-TTF)$_2$KHg(SCN)$_4$: ▲, Q2D AMRO; ■, Q1D AMRO; - - - -, phase boundary of [21].

magnetic field [27]. The special angles θ_i between the axis of the warped Fermi surface cylinder and the magnetic field, at which the Q2D AMRO maxima occur, are given by

$$b'k_\perp \tan\theta_i = \pi(i \pm \tfrac{1}{4}) + A(\phi) \tag{5}$$

where the signs $-$ and $+$ correspond to positive and negative θ_i, respectively, b' is the effective interplanar spacing, $A(\phi)$ is a function of the plane of rotation of the field that is determined by the plane of the Fermi surface warping, $k_\parallel$, is the maximum Fermi wavevector projection on the plane of rotation of the field and $i = \pm 1, \pm 2, \ldots$. Here positive i correspond to $\theta_i > 0$ and negative i to $\theta_i < 0$. Hence from the gradient of a plot such as figure 8(a) the Fermi surface wavevector projection in the plane of rotation of the magnetic field vector may be derived, i.e. rotation at $\phi = 0^\circ$ on our data yields $k_\parallel$ in the $\boldsymbol{a}$ axis direction. The shape of the Fermi surface pocket could thus be mapped out at the points where the azimuthal angle dependence of the Q2D AMROs was recorded.

This analysis has been performed for point B (30 T, 1.4 K) in figure 8(c). If it is assumed that the Fermi surface pocket being studied has an elliptical cross section, then the projection vector $k_\parallel$ (normal to the tangent) is related to the major semiaxis k_x and minor semiaxis k_y of the ellipse by

$$k_\parallel = [k_x^2 \cos^2(\phi - \xi) + k_y^2 \sin^2(\phi - \xi)]^{1/2} \tag{6}$$

where ϕ is again the azimuthal angle describing the angular position in the plane of the ellipse and ξ is the inclination of the major axis with respect to $\phi = 0^\circ$. For an elongated ellipse, equation (6) describes a locus in the form of a figure 'eight' in polar $k_\perp\phi$ space [27], as shown in figure 8(b).

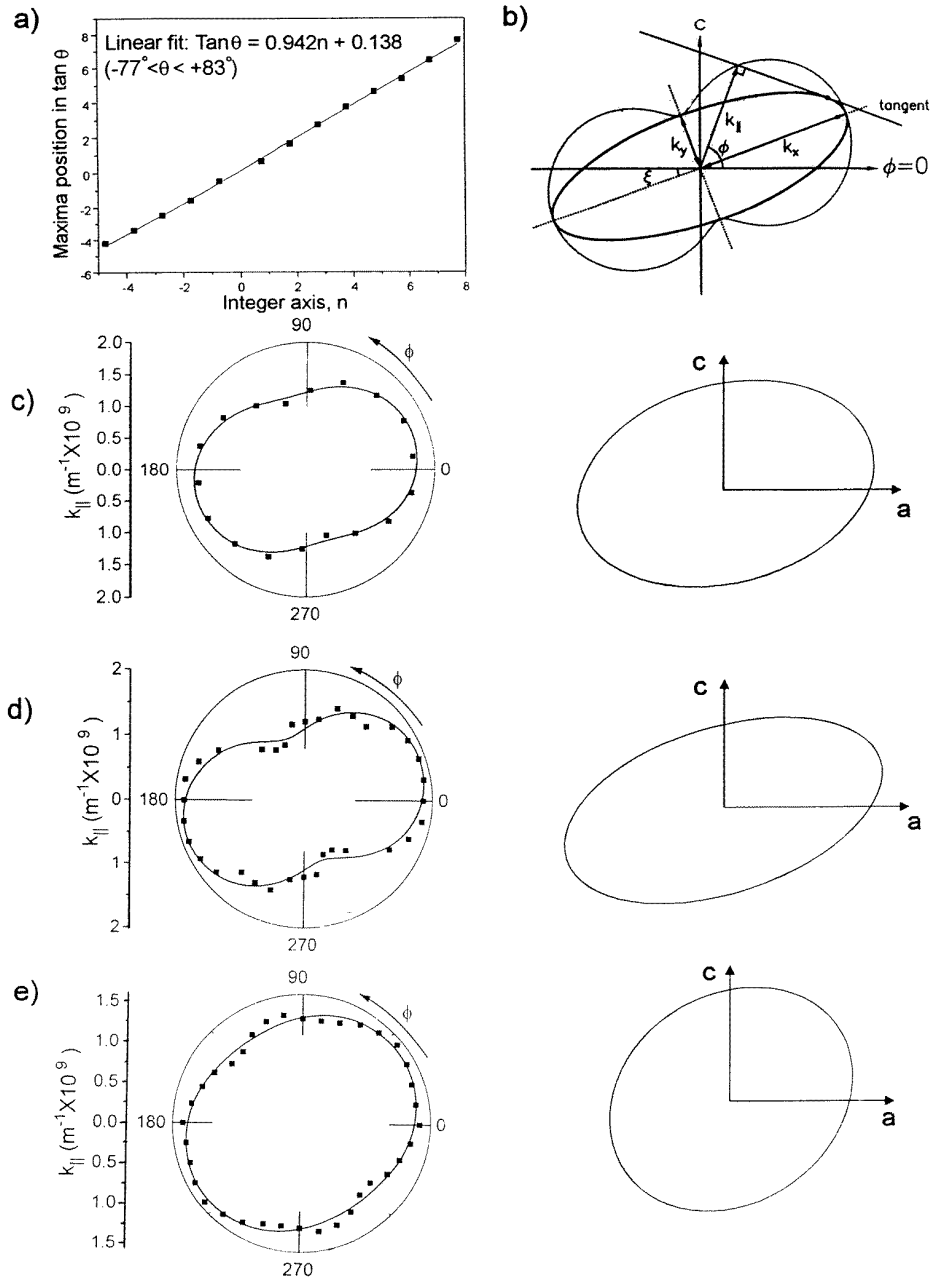

Figure 8. (*a*) A fit of Q2D AMRO peak positions in 30 T α-(BEDT-TTF)$_2$KHg(SCN)$_4$ data to the index n. (*b*) Elliptical Fermi-surface pocket with its associated dumbbell-like locus formed by the callipered width $k_\parallel$ of the ellipse in the complete range of azimuthal angles ϕ. (*c*) Fit to equation (6) and resultant Fermi surface pocket for α-(BEDT-TTF)$_2$KHg(SCN)$_4$ AMROs recorded at 30 T and 1.4 K. (*d*) Fit to equation (6) and resultant Fermi-surface pocket for α-(BEDT-TTF)$_2$KHg(SCN)$_4$ AMROs recorded at 14 T and 7.1 K. (*e*) Fit to equation (6) and resultant Fermi surface pocket for α-(BEDT-TTF)$_2$NH$_4$Hg(SCN)$_4$ AMROs recorded at 30 T and 1.4 K. Note that the data in (*c*)–(*e*) are derived from measurement across a 180° range of ϕ with the application of a symmetry operator.

Equation (6) has been fitted to the data at point B (figure 8(*c*)), giving the major semiaxis of the ellipse, $k_x = (1.75 \pm 0.02) \times 10^9$ m^{-1}, the minor semiaxis of the ellipse, $k_y = (1.17 \pm 0.03) \times 10^9$ m^{-1}, and showing that the major axis makes an angle $\xi = (15 \pm 5)^\circ$ with the crystalline $\boldsymbol{a}$ axis. The size and shape of the pocket associated with this fit are shown to the right of it. The area of the ellipse is thus $S_\alpha = (6.45 \pm 0.21) \times 10^{18}$ m^{-2} which corresponds to $F_\alpha = 676 \pm 22$ T, in good agreement with the observed SdH frequency $F_\alpha = 671 \pm 1$ T [12].

Figure 8(*d*) shows the ϕ-dependence of the Q2D AMROs mapped out for point D (14 T, 7.1 K) which has been driven into the Q2D regime by the increase in temperature. Again equation (6) was fitted to the data. The resultant ellipse was found to have a major semiaxis of $k_x = (1.91 \pm 0.03) \times 10^9$ m^{-1} and a minor semiaxis of $k_y = (0.98 \pm 0.04) \times 10^9$ m^{-1}. The direction of the major axis of the ellipse was along $\xi = (18 \pm 5)^\circ$. The area of this ellipse was found to be $S_\alpha = (5.91 \pm 0.33) \times 10^{18}$ m^{-2}, giving a SdH frequency $F_\alpha = 619 \pm 35$ T.

It is thus apparent that the Fermi surface pocket mapped out at point D has an identical size and orientation to those derived for point B, within experimental error. The orientations of these ellipses are thus in good agreement with earlier high-*temperature* ($T = 8.5$ K) [17] and high-*pressure* ($P > 5$ kbar) [19] measurements of the Q2D AMROs in α-(BEDT-TTF)$_2$KHg(SCN)$_4$ but differ from the orientation that have previously been quoted for high *fields* by Caulfield *et al* [10].

The size and shape of the Q2D AMRO pockets that we have derived in this paper agree well with those derived at 24 T in [10] although they differ in the orientation of the major axis of the ellipse. The field-dependent AMROs of figure 4 show that the orientation of the Fermi surface pocket does not change between 24 and 30 T. This suggests that there may have been an error in the assignment of the azimuthal angles quoted for the ϕ-dependent results of Caulfield *et al* at fields above the kink transition [10].

The AMRO experiments in the present paper therefore provide no evidence for a rearrangement of the Fermi surface of α-(BEDT-TTF)$_2$KHg(SCN)$_4$ between the high-temperature and high-field extremes of the Q2D section of the B–T phase diagram. This implies that the transition induced by raising the temperature and that caused by increasing the applied field are similar in nature.

4.2. α-(BEDT-TTF)$_2$NH$_4$Hg(SCN)$_4$

As mentioned in section 3, the AMROs in α-(BEDT-TTF)$_2$NH$_4$Hg(SCN)$_4$ originate from a single Q2D Fermi surface pocket. The data in figure 6(*b*) were thus fitted with equation (6) as shown in figure 8(*e*). The major semiaxis obtained from this fit was $k_x = (1.49 \pm 0.02) \times 10^9$ m^{-1} with the minor semiaxis $k_y = (1.22 \pm 0.02) \times 10^9$ m^{-1}. This implies a Fermi surface pocket with area corresponding to a SdH frequency $F_\alpha = 597 \pm 35$ T, in agreement with field sweeps which give $F_a = 567 \pm 1$ T [28]. The ellipticity $\varepsilon = |\boldsymbol{k}_x|/|\boldsymbol{k}_y|$, of the Fermi surface pocket in α-(BEDT-TTF)$_2$NH$_4$Hg(SCN)$_4$ is $\varepsilon = 1.22 \pm 0.02$ while, for α-(BEDT-TTF)$_2$KHg(SCN)$_4$, $\varepsilon = 1.49 \pm 0.04$ (at 30 T and 1.4 K). This is partly responsible for a large error in the determination of the orientation of the major axis of the Fermi surface ellipse in α-(BEDT-TTF)$_2$NH$_4$Hg(SCN)$_4$. This is found to be $\xi = (+36 \pm 10)^\circ$. It should be noted the negative $\boldsymbol{a}$ axis and the positive $\boldsymbol{a}$ axis of the crystal could not be distinguished by infrared reflectivity measurements and so there is an arbitrariness in our assignment of the orientation of the major axis of the α-(BEDT-TTF)$_2$NH$_4$Hg(SCN)$_4$ Fermi surface pocket insofar as it might lie along the reflection of ξ about the $\boldsymbol{c}$ axis, i.e. $\xi = (144 \pm 10)^\circ$. This arbitrariness is absent in the α-(BEDT-TTF)$_2$KHg(SCN)$_4$ AMRO data since the agreement

of the orientation of the Q1D Fermi surface sheets in the low-field low-temperature state with that obtained in earlier measurements can in that case be used to assign the $\boldsymbol{a}$ axis direction unambiguously. We shall assume in what follows that $\xi = (36 \pm 10)^\circ$ since this agrees more nearly with the AMROs in the Q2D regime of α-(BEDT-TTF)$_2$KHg(SCN)$_4$ and theoretical predictions of the Fermi surface.

5. Comparison with band-structure calculations

Recently Seo *et al* [29] have carried out extended-Hückel tight-binding band-structure calculations for the α-phase salt structure as a refinement of the original simplified tight-binding method of Oshima *et al* [2] (shown in figure 1(*c*)). These calculations (determined from the 104 K crystal structure) predict a Fermi surface hole pocket centred at the Z point of the Brillouin zone that is tilted just off the Γ–X line in the same sense as the pocket measured in our high-temperature and high-field AMRO study. A comparison of our experimental data with the theoretical predictions of [29] is given in table 1. It is clear that the calculations of Seo *et al* broadly predict the experimental findings of the present work, indicating the validity of their method.

Table 1. Comparison of AMRO results with theoretical band-structure predictions.

	Q2D AMRO result			Band-structure calculation prediction		
Data set	Area (% of area of Brillouin zone)	Ellipticity k_x/k_y	Angle of major axis to $\boldsymbol{a}$ axis (deg)	Area (% of area of Brillouin zone)	Ellipticity k_x/k_y	Angle of major axis to $\boldsymbol{a}$ axis (deg)
α-(BEDT-TTF)$_2$KHg(SCN)$_4$ (30 T, 1.4 K)	16.4 ± 0.5	1.49 ± 0.04	$+15 \pm 5$	12	1.5	+9
α-(BEDT-TTF)$_2$KHg(SCN)$_4$ (14 T, 7.1 K)	15.9 ± 0.9	1.94 ± 0.1	$+18 \pm 5$	12	1.5	+9
α-(BEDT-TTF)$_2$NH$_4$Hg(SCN)$_4$ (30 T, 1.4 K)	14.5 ± 0.9	1.22 ± 0.02	$+36 \pm 10$	10	1.5	+13

In conclusion, in this paper the phase boundary for the change in the AMRO dimensionality in α-(BEDT-TTF)$_2$KHg(SCN)$_4$ has been followed from the low-temperature high-field limit to the low-field high-temperature limit. Measurements within the low-field low-temperature state have shown that the AMROs in this regime result from Q1D Fermi surface sheets aligned at an angle $\phi = (65.7 \pm 1)^\circ$, in agreement with earlier experiments [10, 14, 16, 17]. It has been shown that the form of the AMROs in α-(BEDT-TTF)$_2$KHg(SCN)$_4$ in the 'normal' metallic state is unchanged across that region of the *B–T* phase diagram; these result form a single elliptical hole pocket, tilted at a small positive angle relative to the crystalline $\boldsymbol{a}$ axis. This strongly suggests that the Fermi surface is also unchanged in this region. The shape of the Q2D pocket is found to be similar in the isostructural salt α-(BEDT-TTF)$_2$NH$_4$Hg(SCN)$_4$ and agrees well with the high-pressure AMRO study of [19]. Also, the experimentally determined Fermi surface pocket shapes are found to agree well with recent band-structure calculations [29].

Acknowledgments

We would like to thank Professor M H Whangbo for useful discussions and for communicating to us the results of [29] prior to publication. We would also like to acknowledge Professor D Shoenberg, Professor J S Brooks, Dr S O Hill, Dr M Naughton and Dr S Uji for stimulating discussions. We are grateful to the EPSRC for funding and to Vaughan Williams, Jos Rook, Dennis Rawlings, Robert Harris, Terry Holliday and Dr F L Pratt for expert technical assistance. Portions of this work was performed at the High Field Magnet Laboratory at Nijmegen University, The Netherlands, which is supported by FOM and the EC Large Installations Programme and also at the National High Magnetic Field Laboratory, Tallahassee, which is supported by NSF Co-operative Agreement DMR-9016241 and by the State of Florida.

Note added in proof. Recently, a model purporting to explain the general form of the background magnetoresistance (including the field region in which the kink transition takes place) of the α-(BEDT-TTF)$_2$MHg(SCN)$_4$ (where M = Tl, Rb and K) salts has been published [30]. This model attempts to account for the magnetoresistive behaviour of these materials purely in terms of the magnetic breakdown of a Fermi surface network qualitatively similar to that in figure 1(d) of the present paper. The motivation for pursuing this idea seems merely to be based upon a superficial resemblance of the magnetoresistance observed in the α-phase BEDT-TTF salts (when the magnetic field is perpendicular to the ac-planes) to that seen in magnesium and zinc. It ignores the possibility of any field-induced Fermi surface reconstruction occurring in these materials up to fields as high as 50 T, including at the kink transition. There is now a large body of experimental evidence that refutes the latter underlying assumption of [30] (see section 1 of the present paper and references therein). In particular: (1) The temperature- and field-dependent change in the AMRO dimensionality described in the present work has been clearly associated with the sharp change in the magnetoresistance at the kink, indicating a Fermi surface reconstruction [10, 17–18, 22]. (2) A rapid change in the form of the background magnetoresistance is observed as a function of the tilt angle, θ, of the magnetic field. In particular, the magnetoresistance is 'sublinear' in the first AMRO minimum and has a sharp *increase* upon traversing the kink field at this angle [31, 32]. (3) The observation of high-frequency ($\simeq$ 4270 T) quantum oscillations in the low-field phase that are absent above the kink transition [12, 32] also indicates a Fermi surface reconstruction; in a conventional breakdown network this Fermi surface orbit would be expected to become progressively more dominant in the SdH oscillation spectrum as the field increases. Therefore we believe that [30] is not a valid model for the magnetoresistance of α-phase BEDT-TTF salts.

References

[1] Ishiguro T and Yamaji K 1990 *Organic Superconductors* (Berlin: Springer)
Wosnitza J 1996 *Fermi Surfaces of Low-Dimensional Organic Metals and Superconductors* (Berlin: Springer)
[2] Oshima M, Mori H, Saito G and Oshima K 1989 *Chem. Lett.* **7** 1159
[3] Kushch N D, Buravov L I, Kartsovnik M V, Laukhin V N, Pesotskii S I, Shibaeva R B, Rozenberg L P, Yagbuskii E B and Zvarikina A V 1993 *Synth. Met.* **46** 271
[4] Mori H, Tanaka S, Oshima K, Oshima M and Saito G 1990 *Solid State Commun.* **74** 1261
[5] Mori H, Tanaka S, Oshima M, Saito G, Mori T, Maruyama Y and Inokuchi H 1990 *Bull. Chem. Soc. Japan* **63** 2183
[6] Sasaki T, Toyota N, Tokumoto M, Kinoshita N and Anzai H 1990 *Solid State Commun.* **75** 93
Sasaki T and Toyota N 1992 *Solid State Commun.* **82** 447
Sasaki T, Sato H and Toyota N 1991 *Synth. Met.* **42** 2211
[7] Ito H, Kartsovnik M V, Ishimoto H, Kono K, Mori H, Kushch N D, Saito G, Ishiguro T and Tanaka S 1995 *Synth. Met.* **70** 899
Ito H, Kaneko H, Ishiguro T, Ishimoto H, Kono K, Horiuchi S, Komatsu T and Saito G 1993 *Solid State Commun.* **85** 1005
[8] Pratt F L, Sasaki T and Toyota N 1995 *Phys. Rev. Lett.* **74** 3892
[9] Brooks J S, Agosta C C, Klepper S J, Tokumoto M, Kinoshita N, Anzai H, Uji S, Aoki H, Perel A S, Athas G J and Howe D A 1992 *Phys. Rev. Lett.* **69** 156

[10] Caulfield J, Blundell S J, du Croo de Jongh M S L, Hendriks P T J, Singleton J, Doporto M, Pratt F L, House A, Perenboom J A A J, Hayes W, Kurmoo M and Day P 1995 *Phys. Rev.* B **51** 8325
Caulfield J, Singleton J, Hendriks P T J, Perenboom J A A J, Pratt F L, Doporto M, Hayes W, Kurmoo M and Day P 1994 *J. Phys.: Condens. Matter* **6** L155
[11] Wosnitza J, Crabtree G W, Wang H H, Geiser U, Williams J M and Carlson K D 1992 *Phys. Rev.* B **45** 3018
[12] Harrison N, House A, Deckers I, Caulfield J, Singleton J, Herlach F, Hayes W, Kurmoo M and Day P 1995 *Phys. Rev.* B **52** 5584
[13] Uji S, Terashima T, Aoki H, Tokumoto M, Kinoshita T, Kinoshita N, Tanaka Y and Anzai H 1994 *Physica* B **201** 479
Pratt F L, Singleton J, Doporto M, Fisher A J, Janssen T J B M, Perenboom J A A J, Kurmoo M, Hayes W and Day P 1992 *Phys. Rev.* B **45** 13 904
[14] Kartsovnik M V, Kovalev A E and Kushch N D 1993 *J. Physique I.* **3** 1187
[15] Iye Y, Yagi R, Hanasaki N, Kagoshima S, Mori H, Fujimoto H and Saito G 1994 *J. Phys. Soc. Japan* **63** 674
[16] Kartsovnik M V, Laukhin V N, Pesotskii S I, Schegolev I F and Yakovenko V M 1991 *J. Physique I.* **2** 89
Yamaji K 1989 *J. Phys. Soc. Japan* **58** 1520
[17] Kovalev A E, Kartsovnik M V, Shibaeva R P, Rozenberg L P, Schegolev I F and Kushch N D 1994 *Solid State Commun.* **89** 575
[18] Sasaki T and Toyota N 1994 *Phys. Rev.* B **49** 10 120
[19] Hanasaki N, Kagoshima S, Miura N and Saito G 1996 *J. Phys. Soc. Japan* **65** 1010
[20] Brooks J S, Chen X, Klepper S J, Valfells S, Athas G J, Tanaka Y, Kinoshita T, Kinoshita N, Tokumoto M, Anzai H and Agosta C C 1995 *Phys. Rev.* B **52** 14 457
[21] Sasaki T and Toyota N 1992 *Solid State Commun.* **82** 447
[22] Kartsovnik M V, Kovalev A E, Laukhin V N, Schegolev I F, Ito H, Ishiguro T, Kushch N D, Mori H and Saito G 1995 *Synth. Met.* **70** 811
[23] Oshima M, Mori H, Saito G and Oshima K 1989 *Chem. Lett.* **7** 1159
[24] Pratt F L, Hayes W, Fisher A J, Singleton J, Spermon S J R M, Kurmoo M and Day P 1989 *Synth. Met.* **29** F667
Kuroda H, Yakushi K, Tajima H, Ugawa A, Tamura M, Okawa Y, Kobyashi A, Kato R, Kobyashi H and Saito G 1988 *Synth. Met.* **27** A491
[25] Lebed A G 1986 *JETP Lett.* **43** 174; 1994 *J. Physique I* **4** 351; 1995 *Synth. Met.* **70** 993
Lebed A G and Bak P 1989 *Phys. Rev. Lett.* **63** 1315
Strong S P, Clarke D G and Anderson P W 1994 *Phys. Rev. Lett.* **73** 1007
Osada T, Kagoshima S and Miura N 1992 *Phys. Rev.* B **46** 1812
Chaikin P M 1992 *Phys. Rev. Lett.* **69** 2831
Maki K 1992 *Phys. Rev.* B **45** 5111
[26] Blundell S J and Singleton J 1996 *Phys. Rev.* B **53** 5609
[27] House A A, Harrison N, Blundell S J, Deckers I, Singleton J, Herlach F, Hayes W, Perenboom J A A J, Kurmoo M and Day P 1996 *Phys. Rev.* B **53** 9127
[28] Wosnitza J, Crabtree G W, Wang H H, Geiser U, Williams J M, and Carlson K D 1992 *Phys. Rev.* B **45** 3018
[29] Seo D-K, Whangbo M-H, Fravel B and Montgomery L K 1996 *Solid State Commun.* **100** 191
[30] McKenzie R H, Athas G J, Brooks J S, Clark R G, Dzurak A S, Newbury R, Starrett R P, Skougarevsky A, Tokumoto M, Kinoshita N, Kinoshita T and Tanaka Y 1996 *Phys. Rev.* B **54** R8289
[31] Athas G J, Brooks J S, Valfells S, Klepper S J, Tokumoto M, Kinoshita N, Kinoshita T and Tanaka Y 1994 *Phys. Rev.* B **50** 17 713
[32] House A A, Haworth C J, Caulfield J M, Blundell S J, Honold M M, Singleton J, Hayes W, Hayden S M, Meeson P, Springford M, Kurmoo M and Day P 1996 *J. Phys.: Condens. Matter* to be published